Enhancement of Mechanical Q Factors by Optical Trapping

K.-K. Ni, R. Norte, D. J. Wilson, J. D. Hood, D. E. Chang, O. Painter, and H. J. Kimble

Enhancement of mechanical Q-factors by optical trapping

K.-K. Ni[1], R. Norte[2], D. J. Wilson[1], J. D. Hood[1], D. E. Chang[1,3], O. Painter[2], and H. J. Kimble[1]

[1] Norman Bridge Laboratory of Physics 12-33, California Institute of Technology, Pasadena, CA 91125

[2] T. J. Watson, Laboratory of Applied Physics, California Institute of Technology, Pasadena, CA 91125 and

[3] ICFO - Institut de Ciences Fotoniques, Mediterranean Technology Park, 08860 Castelldefels, Barcelona, Spain

The quality factor of a mechanical resonator is an important figure of merit for various sensing applications and for observing quantum behavior. Here, we demonstrate a technique to push the quality factor of a micro-mechanical resonator beyond conventional material and fabrication limits by using an optical field to stiffen or "trap" a particular motional mode. Optical forces increase the oscillation frequency by storing most of the mechanical energy in a nearly lossless optical potential, thereby strongly diluting the effect of material dissipation. By using a 130 nm thick SiO_2 disk as a suspended pendulum, we achieve an increase in the pendulum center-of-mass frequency from 6.2 kHz to 145 kHz. The corresponding quality factor increases 50-fold from its intrinsic value to a final value of $Q = 5.8(1.1) \times 10^5$, representing more than an order of magnitude improvement over the conventional limits of SiO_2 for this geometry. Our technique may enable new opportunities for mechanical sensing and facilitate observations of quantum behavior in this class of mechanical systems.

PACS numbers:

Mechanical resonators are widely used as exquisite sensors of weak perturbations such as small forces [1, 2], displacements [3, 4], and changes in mass [5, 6]. In fact, a number of systems have advanced to the point that it is possible to detect quantum effects in their motion [4, 7–9], raising the exciting possibility that such systems might eventually lead to applications in quantum information processing [10–12] and the observation of quantum effects at macroscopic scales [13, 14].

The performance of a mechanical resonator depends critically on its quality factor, which characterizes both the maximum response of an oscillator to a disturbance at its resonance frequency (signal) and the coupling rate to its surrounding dissipative environment (noise). Improving quality factors beyond state-of-the-art parameters is a challenging task since a number of systems are now limited by fundamental dissipation mechanisms, e.g. thermoelastic damping [15] and internal friction [16].

In this Letter, we experimentally demonstrate a technique that enables the quality factor of a mechanical system to be enhanced beyond conventional material limits. Our technique involves optically trapping a thin, dielectric membrane whose geometry is designed so that the natural material forces are extremely weak [17]. In this limit, almost all mechanical energy is stored in an ultralow loss potential provided by strong optical restoring forces, which dilute the effects of internal material dissipation [17, 18]. The trapped oscillator is analogous to a mechanical oscillator with a spring that is stiffen by increased mechanical tensile stress [19–21] in that both the oscillator frequency and the Q increase. Our general scheme is implemented for a particular example of an SiO_2 dielectric disk supported by a single thin tether, trapped in an optical standing wave. We observe an increase in the "pendulum" mode frequency from 6.2 kHz to 145 kHz as the optical power is increased, leading to a final quality factor of $Q_f = 5.8(1.1) \times 10^5$. Q_f represents greater than fifty-fold increase over the intrinsic Q_i of our device in the absence of optical trapping forces, and significantly, more than an order of magnitude improvement over estimates of the conventional dissipative rate of our SiO_2 disk [22, 23]. These results substantiate the potential of our technique to facilitate mechanical sensors with enhanced sensitivity and quantum devices based upon mechanical systems.

Optical forces are generally feeble as compared to mechanical forces, which makes optical manipulation of mechanical oscillators challenging. To implement optical trapping of membranes, we begin by fabricating a nearly free-standing dielectric film in a pendulum geometry. We chose SiO_2 as the membrane material mainly for its low optical absorption [24]. The pendulum (Fig. 1) consists of a 10 μm diameter disk held by a 50 μm × 0.43 μm tether, which is attached to a large, square annulus of SiO_2 that has a width of $\sim$ 60 μm. The thickness of all the suspended parts (i.e. the disk, the tether, and the annulus) is 130 nm.

To investigate properties related to a trapped pendulum, we load the 1×1 cm pendulum chip, which typically contains a dozen devices, into a vacuum chamber traversed by an optical standing wave. A schematic of the experimental setup is shown in Fig. 2(A). The pendulums hang vertically inside the chamber, which is evacuated to a pressure below 10^{-7} mbar to make gas damping negligible. The optical standing wave is formed by a retro-reflected Gaussian beam, which has been focused to a $1/e^2$ waist $\omega_0 \simeq 17$ μm at the position of the disk. The trap beam is derived from a high power Nd:YAG laser operating at a wavelength of $\lambda =$1.064 μm. We vary the incident laser power between 3 mW to 17 W using a waveplate and a polarizing cube. The centering of the trap beam on the pendulum disk is critical for achieving large trapping potentials without mixing "center-of-mass" (CM) motion of the pendulum with vi-
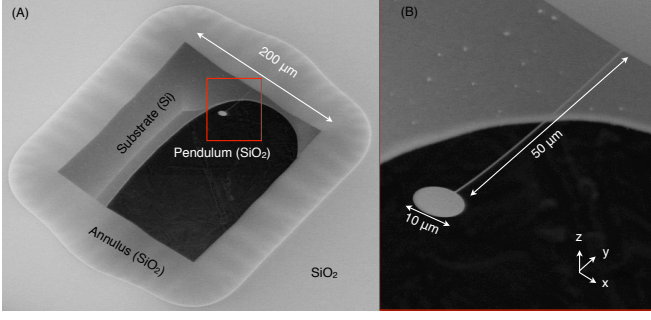
FIG. 1: Scanning electron micrographs of the device: a 130 nm thick SiO_2 membrane forms the pendulum, which consists of a 10 μm diameter disk and a 50 μm $\times$ 0.43 μm tether. (A) Overview: The pendulum is suspended from a 60 μm wide SiO_2 annulus. The annulus (wrinkled area) and the pendulum are etched into a SiO_2 film for which the Si substrate directly underneath has been removed. The dark background in the center is a clear opening of the substrate. (B) Close-up view of the pendulum, which is deflected 10-15 degrees out of the plane of the substrate due to residual stress of the film.
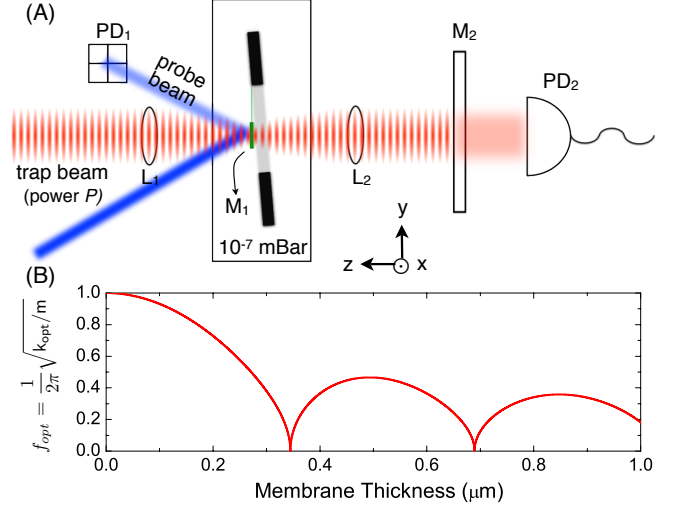

FIG. 2: Optical trapping of a membrane disk. (A) Schematic of the experimental setup. The membrane chip is enclosed inside a vacuum chamber. We trap the disk in an optical standing wave formed by a single laser beam at 1.064 μm and its reflection from the disk (M_1) and a mirror (M_2, reflectivity = 0.98). We monitor the thermal motion of the pendulum by the deflection of an off-axis probe beam (blue) reflected from the disk onto a quadrant photodiode (PD_1) and transmitted intensity onto PD_2. (B) Calculated trap frequency f_{opt} vs membrane thickness d_m normalized to f_{opt} at $d_m/\lambda \to 0$ for a fixed optical power. For $d_m \sim \lambda$, we solve for the steady electric-field amplitude on the left and right of the membrane.

brational modes of the tether. This degree of freedom is carefully aligned by monitoring transmission of the forward and retro-reflected beams through the disk. In addition, to ensure that the disk is perpendicular to the optical standing wave, we implement a pair of actuators to tip and tilt the chip to prevent the pendulum from settling into a configuration in which the disk extends over multiple periods of the standing wave.

For the optical standing wave configuration shown schematically in Fig. 2(A), we estimate the trapping potential by balancing expressions for the radiation pressure force on either side of the membrane. To simplify the problem, we assume that the disk is infinitely stiff, that it is free to move along the axis of the trap, and that the incident optical beam is smaller than the disk so that diffraction from the edges may be ignored. We solve for the electric-field of a single beam in the presence of two reflectors, M_1(the disk) and M_2, as a function of the membrane thickness, d_m. Stable equilibria occur at the positions where the force between the incoming beam and the finite electric field built up between M_1 and M_2 are balanced, which are neither at nodes nor anti-nodes of the standing wave. At each equilibrium position, the optical spring constant of the trap is $k_{opt} = \frac{16\pi}{\lambda} \frac{|r_m|}{|t_m|} \frac{P}{c}$, where P is the incoming power, r_m and t_m are the reflectance and the transmittance of the membrane determined by d_m and the index of refraction of the film [25], and c is the speed of light. In Fig. 2(B), we plot the calculated optical trapping frequency, $f_{opt} = \frac{\sqrt{k_{opt}/m}}{2\pi}$, normalized to the prediction for a membrane with $d_m/\lambda \to 0$. For our membrane with thickness $d_m = 0.13\,\mu$m, the trapping frequency is 88% of the value predicted for a membrane with $d_m/\lambda \to 0$. It is interesting to note that the optical spring constant for a membrane in the middle of a high finesse Fabry-Perot cavity is also $k_{opt} = \frac{16\pi}{\lambda} \frac{|r_m|}{|t_m|} \frac{P}{c}$, where

P is now the circulating power. In this case, however, the membrane center would be trapped specifically at either an anti-node or a node of the standing wave depending on the membrane thickness.

Intrinsic vibrational modes and frequencies of the pendulum structure are probed by reflecting an independent "probe" beam ($\lambda = 0.852\,\mu$m) from the disk at an oblique angle (50°) with respect to the trap. The reflected beam is directed to a quadrant photodiode (PD_1) [26] which is calibrated using the membrane tip/tilt actuators. The quadrant photodiode can be split into two horizontal pairs of sensors ("top" and "bottom") and two vertical pairs of sensors ("left" and "right"). Analysis is performed on the difference between the "top" and "bottom" combined photosignals (expressed as a transimpedance-amplified photocurrent, $V_{TB}(t)$) and the difference between the "left" and "right" combined signals ($V_{LR}(t)$). Fourier transforms of $V_{TB}(t)$ and $V_{LR}(t)$ reveal the frequencies and tip/tilt orientation of the vibrational modes (Fig. 3(A)). We identify low-order vibrational modes by comparison of the observed frequency spectrum and their characteristic mode shapes to a finite-element simulation (Fig. 3(B), COMSOL 3.5a) based on the membrane material properties and its geometry measured using a scanning electron microscope. We see approximately a factor of two discrepancy in the simulated frequencies versus measurements in the absence of optical forces. This is
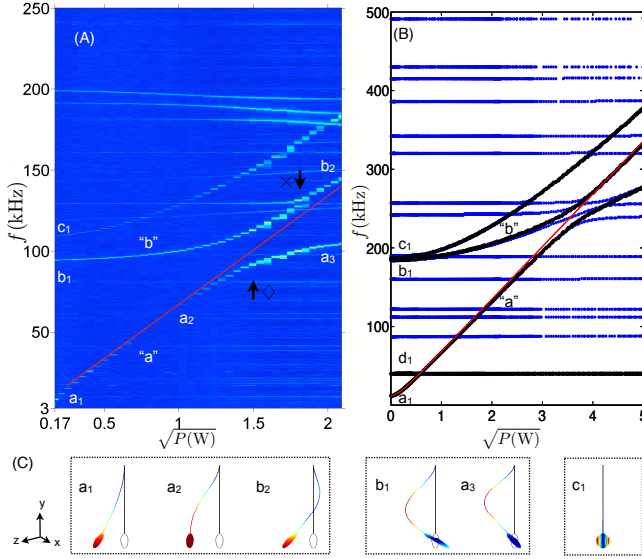
FIG. 3: Displacement power spectrum of vibrational modes. (A) Spectrogram of vertical angular displacement (inferred from deflection measurement, Fig. 2(A)) versus trapping power, P. Several vibrational mode branches are evident, e.g. "a" and "b". As the optical trap power is increased (in discrete steps), the frequencies of the three lowest modes (a_1, b_1, c_1) increase as $\sqrt{f_{0i}^2 + \alpha_i \cdot P}$ (see text). Two avoided crossings are visible here: ($\diamond$) formed by the CM mode and the violin mode; ($\times$) formed by the CM mode and an annulus mode. At higher powers, the CM mode is a hybrid of pendulum and violin motion (b_2). Other visible modes in the spectrum are associated with vibrations of the annulus. Overall, the CM frequency shifts from 6.2 kHz to 145 kHz when 4.3 W of optical power is applied. (B) Finite-element simulated spectrum of an optically trapped pendulum (black) suspended from an annulus (blue) that is in turn anchored to a substrate (as in Fig. 1(a)) for qualitative comparison to (A). The red lines in both (A) and (B) are drawn for a trapping slope of $\alpha = 4500 \frac{\text{kHz}^2}{\text{W}}$. (C) Simulated mode shapes for different optical trapping forces in (A). (a_1) the "pendulum" mode, also called the "CM" mode, (b_1) the "violin" mode, and (c_1) the "torsional" mode.

most likely due to an overestimate of the Young's modulus for the very thin SiO_2 layer where surface effects can be important. The mode shapes in the absence of optical forces calculated from simulation are illustrated in Fig. 3(C) as (a_1) the "pendulum" mode, also called the "CM" mode, where the pendulum disk swings along the axis of the trapping beam ($f_{0a} = 6.2$ kHz), (b_1) the "violin" mode ($f_{0b} = 93$ kHz), and (c_1) the "torsional" mode ($f_{0c} = 109$ kHz). One additional mode that is not shown in the figure is (d_1) the transverse pendulum mode swinging orthogonal to the axis of the trapping beam (25 kHz). We are most interested in the CM mode because it exhibits the least mechanical deformation which leads to energy dissipation [17].

In the presence of an optical trap, the frequency of the membrane is determined by the sum of the optical restor-

ing force and the intrinsic mechanical restoring force. The contribution from gravity is small (< 100 Hz) and is neglected. The trap is first aligned at a low trapping power (3 mW). To ensure that the tether does not provide a significant initial restoring force, we also fine tune the trapping laser wavelength so that the equilibrium position of the trap coincides with the natural axial position of the membrane. We diagnose their coincidence by minimizing the vertical deflection of the probe beam (evident in the mean value of V_{TB}) when the trap is turned on. Figure 3(A) shows the power spectrum of V_{TB}, which reflects the vertical angular displacement of the pendulum, as a function of trap power, P. For comparison, we show a spectrum generated by a finite element model (Fig. 3(B)) that treats the optical trap as a restoring force with a Gaussian transverse profile. Close comparison of the observed and model spectra adds to our understanding of several distinct features. As the optical trap power is increased, the frequencies of the three lowest visible modes increase as $\sqrt{f_{0i}^2 + \alpha_i \cdot P}$, where f_{0i} represents their natural frequency and α_i is the trapping slope coefficient for each mode. As the CM mode frequency increases, the mode shape also changes via the bending of the tether. This change is first evident in the reduction of the CM mode signal near 50 - 75 kHz. The reduction occurs as the mode shape changes from Fig. 3(C, a_1) to (C, a_2), which to first order does not deflect vertically. In addition, as expected, we do not see such a reduction for corresponding trapping beam transmission on PD_2 (not displayed) that probes pure axial disk displacement. The mode shape again changes as the CM mode and the violin mode (Fig. 3(C, b_1)) form an avoided crossing near 93 kHz. At higher power, the CM mode is a hybrid of pendulum and violin modes (Fig. 3(C, b_2)). As the frequency continues to increase, the CM mode crosses an annulus mode. Overall, the CM mode frequency shifts from 6.2 kHz to 145 kHz when 4.3 W of optical power is applied, corresponding to a trapping slope coefficient of $\alpha_{CM} = 4880\,\text{kHz}^2/\text{W}$, in good agreement with the simulated value of $\alpha_{CM}^{FEM} = 4500\,\text{kHz}^2/\text{W}$ (the inferred value from measurement being overestimated due to the mode anti-crossing). At trapping powers greater than 4.3 W, we find that the CM frequency ($f = 145$ kHz) is near yet another vibrational mode of the annulus. With further increases in power, the large thermal displacements of the annulus mode greatly dominates the motion of the CM pendulum mode, making it difficult to identify.

One of the most important consequences of optical trapping is an increase of the mechanical Q [17]. The large increase in frequency of the CM mode through optical trapping implies that the amount of mechanical energy stored in the optical fields U_o dominates over that stored in internal stresses, U_m. Because the optical potential is nearly lossless due to the low optical absorption of SiO_2 [24], the effects of material dissipation are diluted by a factor $U_m/(U_o + U_m)$. Therefore, we would expect the mechanical Q of the system to increase as the inverse of the dilution factor $\sim U_o/U_m$ for a
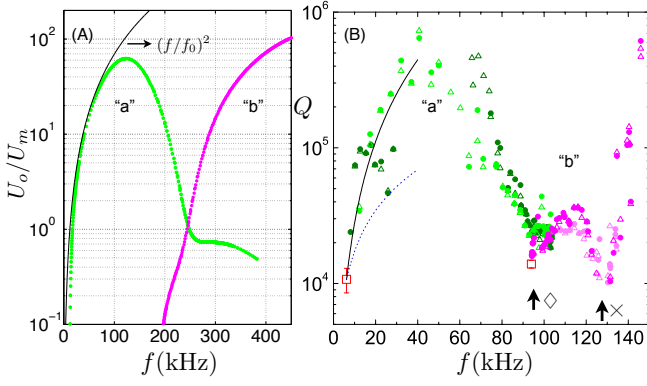
FIG. 4: Mechanical Q-factor of the trapped pendulum. (A) Finite-element calculation of the ratio between the energy stored in the optical potential (U_o) and the mechanical potential (U_m) vs trap frequency. The two branches corresponding to "a" and "b" vibrational modes respectively in Fig. 3. (B) Q vs trapping frequency for two vibrational modes in the trap, independently recorded on PD$_1$ (circles) and PD$_2$ (triangles). In addition, two dataset with slightly different optical trapping alignments are shown for "a" (light and dark green) and "b" (light and dark magenta). The Q of the CM mode increases 60-fold from its natural value, $Q_i = 1.1(2) \cdot 10^4$ ($P = 0$, data in red square) with a slope that is consistent with $(f/f_0)^2$ scaling (solid line) before turning over near the avoided crossing ($\diamond$) with a violin mode. Beyond this avoided crossing, Q increases again followed by a minimum near the annulus avoided-crossing ($\times$) and then a steep increase. We also show the expectation of a Q-increase that scales as f/f_0 (dashed line) for comparison. We find the measured Q increase to be in qualitative agreement with the calculated $1 + \frac{U_o}{U_m}$ in (A).

frequency-independent damping mechanism. For an ideal system, one would find an indefinite increase in the ratio $U_o/U_m = (f/f_0)^2$ with increasing trap power. In practice, this ratio saturates due to factors such as the mass ratio between the trapped disk and the untrapped tether, the mode mixing with the modes of the support structure (tether and annulus in our case), and induced mechanical strain due to an inhomogeneous trapping beam profile [17]. Accounting for these effects, our finite-element simulation predicts a maximum of $U_o/U_m \sim 100$ (see Fig. 4(A)) in our experimentally achievable frequency range. Further improvement on reduction of the tether width will increase the U_o/U_m ratio.

To infer the Q of the trapped pendulum, we record the thermal motion $X(t) \propto V_{TB}(t)$ at each laser power for a few minutes and numerically compute the energy auto-correlation, $R_E(\tau) \equiv \langle X(t)^2 X(t + \tau)^2 \rangle$, over a Fourier frequency range encompassing the mechanical frequency [27]. For a high Q oscillator driven by Gaussian thermal noise, $R_E(\tau)$ is characterized by an exponential decay with time constant τ_E, in correspondence to our measurements and relates to the mechanical quality factor by $Q = 2\pi f \tau_E$. We verify our oscillator is driven by thermal energy by comparing the pendulum disk angular

displacement energy in the absence of the optical trap to the expected thermal energy at 300 K and find the agreement to be within 20%. This agreement rules other technical noise drives such as seismic noise or beam pointing noise insignificant. The pendulum in the absence of trapping forces has an initial value $Q_i = 1.1(2) \times 10^4$ and a 20% deviation from shot to shot.

A summary of our Q-measurement results is presented in Fig. 4(B). We compare the result of monitoring vertical angular displacement of the pendulum on PD$_1$ (data in circles) with the result of monitoring axial displacement of the pendulum via the trap beam transmission through M$_2$ on PD$_2$ (triangles). The results are consistent in both cases. We observe that the initial Q increase to a maximum value $Q_a = 6.9(1.4) \times 10^5$ is consistent with the $(f/f_0)^2$ scaling and which is in contrast with the stress induced Q-increase studied in SiN nanostrings [19–21]. After the initial increase, Q then drops as the CM mode crosses the violin mode, which is a consequence of an increase of the strain energy in the bending of the tether [17]. Beyond the avoided crossing with the violin mode and a subsequent annulus mode (arrow $\times$), the Q of the CM mode increases again by a factor of > 50 relative to Q_i to a final value $Q_f = 5.8(1.1) \times 10^5$. The dependence of Q on frequency is in qualitative agreement with the calculated U_o/U_m in Fig. 4(A). Overall, we demonstrate that by adding optical energy but not dissipation into the system, we can increase the mechanical Q by more than an order of magnitude.

We expect that further significant advances can be made with refined fabrication techniques and a shift to materials with better mechanical characteristics. For instance, the mechanical frequency and the corresponding Q-factor of our trapped pendulum is limited in part by the large suspended annulus to which the tether is attached (Fig. 1). Using wet chemical anisotropic etching of Si to release the pendulum, it should be possible to fabricate a device with an annulus less than 10 μm wide. Furthermore, while SiO$_2$ proved to be convenient to work with initially, it suffers a relatively low intrinsic quality factor of $Q_i \sim 10^4$ that is likely to be limited by surface-related damping mechanisms [22, 23]. Although the nature of surface damping is still an open question and not necessarily a fundamental limitation, we can still compare our observed Q_i to other SiO$_2$ devices. From the extensive phenomenological study of SiO$_2$ loss angle [23] and the surface-to-volume ratio of our pendulum, we would expect $Q_i \sim 9200$, which is consistent with our observation of $Q_i \approx 1.1 \times 10^4$. Switching platforms to stressed silicon nitride or crystalline silicon should enable material quality factors of $Q_i \sim 10^5$-10^7 [28–30]. In initial experiments with Si$_3$N$_4$, for example, we have fabricated stressed, tethered structures (similar to [31]) with bare frequencies of 172 kHz and $Q_i \sim 1.3 \cdot 10^7$. We expect that by applying optical trapping to such structures, final quality factors of $Q_f \sim 10^8$ might be possible for oscillator frequency ~ 1 MHz. Such values would be unprecedented for any fabricated nano- or micro-mechanical sys-

tem, and remarkably, would be competitive with the prediction for untethered levitated nano-particles [32–36].

Our technique holds promise as a tool to reduce the role of mechanical dissipation in a wide variety of sensing applications as well as in the emerging field of quantum opto-mechanics [37]. Our device can be integrated into a high-finesse cavity employing the "membrane-in-the-middle" geometry [30, 38], for example, and could provide the long coherence times necessary to observe quantum behaviors (i.e., macroscopic entanglement) in a room temperature environment [13, 14]. This work reveals a fascinating new aspect of the interplay between motion and light [39] and should stimulate further exploration.

[1] J. K. Hoskins, et al., Phys. Rev. D **32**, 3084 (1985).
[2] H. J. Mamin and D. Rugar, Appl. Phys. Lett. **79**, 3358 (2001).
[3] A. Abramovici, et al., Science **256**, 325 (1992).
[4] J. D. Teufel, et al., Nat. Nanotechnol. **4**, 820 (2009).
[5] N. V. Lavrik and P. G. Datskos, Appl. Phys. Lett. **82**, 2697 (2003).
[6] T. Ono, et al., Rev. Sci. Instr. **74**, 1240 (2003).
[7] T. Rocheleau, et al., Nature **463**, 72 (2010).
[8] A. D. O'Connell, et al., et al., Nature **464**, 697 (2010).
[9] J. Chan, et al., Nature **478**, 89 (2011).
[10] K. Stannigel, et al., Phys. Rev. Lett. **105**, 220501 (2010).
[11] D. E. Chang, et al., New Journal of Physics **13**, 023003 (2011).
[12] C. A. Regal and K. W. Lehnert, Journal of Physics: Conference Series **264**, 012025 (2011).
[13] C. Genes, et al., New J. Phys. **10**, 095009 (2008).
[14] H. Müller-Ebhardt, et al., Phys. Rev. Lett. **100**, 013601 (2008).
[15] R. Lifshitz and M. L. Roukes, Phys. Rev. B **61**, 5600 (2000).
[16] R. O. Pohl, et al., Rev. Mod. Phys. **74**, 991 (2002).
[17] D. E. Chang, et al., ArXiv e-prints (2011), 1101.0146.
[18] G. Cagnoli, et al., Phys. Lett. A **272**, 39 (2000).
[19] S. S. Verbridge, et al., Nano Letters **7**, 1728 (2007).
[20] Q. P. Unterreithmeier, et al., Phys. Rev. Lett. **105**, 027205 (2010).
[21] S. Schmid, et al., Phys. Rev. B **84**, 165307 (2011).
[22] K. Yasumura, et al., Journal of Microelectromechanical Systems **9**, 117 (2000).
[23] S. D. Penn, et al., Phys. Lett. A **352**, 3 (2006).
[24] D. K. Armani, et al., Nature **421**, 925 (2003).
[25] E. Hecht, *Optics* (Addison-Wesley, 1987), p. 375.
[26] K. Usami, et al., Nat. Phys. **8**, 168 (2012).
[27] B. C. Stipe, et al., Phys. Rev. Lett. **87**, 096801 (2001).
[28] J. Yang, et al., Appl. Phys. Lett. **77**, 3860 (2000).
[29] S. S. Verbridge, et al., J. Appl. Phys. **99**, 124304 (2006).
[30] D. J. Wilson, et al., Phys. Rev. Lett. **103**, 207204 (2009).
[31] D. Kleckner, et al., Opt. Express **19**, 19708 (2011).
[32] A. Ashkin and J. M. Dziedzic, Appl. Phys. Lett. **28**, 333 (1976).
[33] K. G. Libbrecht and E. D. Black, Phys. Lett. A **321**, 99 (2004).
[34] D. E. Chang, et al., Proc. Natl. Acad. Sci. USA **107**, 1005 (2010).
[35] O. Romero-Isart, et al., New J. Phys. **12**, 033015 (2010).
[36] T. Li, et al., Science **328**, 1673 (2010).
[37] M. Aspelmeyer, et al., J. Opt. Soc. Am. B **27**, A189 (2010).
[38] J. D. Thompson, et al., Nature **452**, 72 (2008).
[39] V. B. Braginsky, F. Y. Khalili, and K. S. Thorne, *Quantum measurement* (Cambridge Univ. Press., 1999).